Nano World Journal

https://doi.org/10.17756/nwj.2023-s3-129

Research Article

Open Access

Microstructure of Iron Based Non-equiatomic Alloys Using Laser Cladding Deposition Technique

Pramod G. Musrif[1], P Satishkumar[2*], Balam Durga Prasad[3], Sugumari Vallinayagam[4], Rajasekaran Saminathan[5], B Vishnu Vardhana Naidu[6] and Sai Nandhini Ravi[7]

[1]*AISSMS, Institute of Information Technology, Pune, India*
[2]*Department of Mechanical Engineering, Rathinam Technical Campus, Coimbatore, Tamil Nadu, India*
[3]*Department of Mechanical Engineering, Sagi Rama Krishnam Raju Engineering College, Bhimavaram, Andhra Pradesh, India*
[4]*Department of Biotechnology, Vel Tech Rangarajan Dr. Sagunthala R&D Institute of Science and Technology, Chennai, India*
[5]*Department of Mechanical Engineering, College of Engineering and Computer Science, Jazan University, Saudi Arabia*
[6]*Dept. of Mechanical Engineering, Sree Vidyanikethan Engineering College, Mohan Babu University, Andhra Pradesh, India*
[7]*Department of Biotechnology, Vel Tech Rangarajan Dr. Sagunthala R and D Institute of Science and Technology, Chennai, Tamil Nadu, India*

***Correspondence to:**
P Satishkumar,
Department of Mechanical Engineering,
Rathinam Technical Campus,
Coimbatore, Tamil Nadu, India.
E-mail: sp.sathishkumar10@gmail.com

Received: July 31, 2023
Accepted: October 30, 2023
Published: November 01, 2023

Citation: Musrif PG, Satishkumar P, Prasad BD, Vallinayagam S, Saminathan R, et al. 2023. Microstructure of Iron Based Non-equiatomic Alloys Using Laser Cladding Deposition Technique. *NanoWorld J* 9(S3): S728-S732.

Published by United Scientific Group

Abstract

The research paper focuses on the study of mechanical properties and microstructural analysis of SS316L coated material. The effect of different percentages of boron and tungsten carbide in the range of 7%, 11%, and 15% for boron and 13%, 9%, and 5% for tungsten carbide in iron-based alloys have been used to study erosion wear. The alloys with different composition have been prepared using laser cladding technique. The authors have also carried out the micro-analysis of the alloys using energy dispersive X-ray (EDX) spectroscopy and X-ray photoelectron spectroscopy (XPS) in the current study. In all cases it is observed that addition of these materials increases the mechanical strength and thus improves the wear resistance of the base material. Besides it is also seen that the processes used for cladding these materials improves the corrosion resistance as well.

Keywords

Iron based alloy, Erosive wear, Laser cladding, SS316L

Introduction

The main component used for generating hydropower is a turbine which has blades on which the water flows causing wear and tear of the blades. To withstand wear and tear of the blade from flowing water these blades have to resist the dynamic forces. This requires that the material of the turbine should have good wear resistance, corrosive resistance, erosive resistance, and also high strength to work under the impact of the flowing water. It is already established that erosion is caused mainly due to the erodent particles found as solid particulate in flowing water. Further the type, size, velocity of flow and the angle at which impinges on the blade also are found to be responsible for the erosion of the material.

Nair et al. [1] and Lin et al. [2] have shown that the adverse effect of erosive particles can be greatly reduced by using exterior coating on the base material. The surface or exterior coating not only helps to minimize the effect of corrosion and erosion, but it also improves the service life of the component used in hydro turbines. Thakur et al. [3] have shown that coating of the composite alloys prepared by mixing a number of say four to five elements can have a significant effect on the base material. These composites can be made of metal matrix or plastic matrix; however, composites make from metal matrix has created lot of interests among the researchers because of its higher stiffness value, fracture toughness value, wear and improved corrosion strength. It is also established that the metal

matrix has the capacity to withstand high temperature environment. Sharma et al. [4] have shown that the metal matrix prepared from high entropy alloys can be of equiatomic as well as non-equiatomic in form. Many techniques have been used for coating composites and one of the most common ones for deposition is thermal spraying by [5], physical and chemical vapor deposition by [6, 7]. Leech [8] has shown that laser technologies have also been used due to the high energy density, better consistency, for surface modification of the materials. Some of the laser technologies used for surface analysis are laser peening [9, 10], laser cladding and laser remelting [11, 12], etc. Among all laser technologies, laser cladding is a very effective technology in which cladding powder speedily melts and crystallized on the substrate. Wang et al. [13] and Zhou et al. [14] have shown that laser cladding forms fine grains and strong coating on the surface of the base metal. Laser cladding also gives good metallurgical bond, the infusion rate and the area of heat affected on the substrate is also minimum. It is also shown by Li et al. [15] and Liu et al. [16] that the process improves the wear resistance. Majumdar et al. [17] has shown that laser cladding is environmentally friendly, easy to operate, and wastage of material is also less.

Materials and Method

In the present paper the authors have attempted to study the non-equimolar high entropy alloys $Fe_{50}Mn_{30}Co_{10}Cr_{10}$ alloy that has been prepared by vacuum-induction melted and given the thermos mechanical treatments. In this composition, boron is added to promote the formation of eutectic phase. This eutectic phase helps in improving the microhardness of the substrate as shown by Li et al. [18]. Apart from this, Li et al. [19] has shown that the $Fe_{80-x}Mn_xCo_{10}Cr_{10}$ (with values of x = 45, 40, 35, and 30%) showed a partial athermal martensitic transformation from face-centered cubic (fcc) to hexagonal closest packed (hcp) due to a reduction of the thermal stability of the fcc phase.

In this study, non-equiatomic alloys $Fe_{43}Mb_{15}Cr_{12}Ni_{10}$ with the addition of different percentages of boron and tungsten carbide have been used. Three compositions that have been formed which are $Fe_{43}Mb_{15}Cr_{12}Ni_{10}B_7WC_{13}$, $Fe_{43}Mb_{15}Cr_{12}Ni_{10}B_{11}WC_9$, and $Fe_{43}Mb_{15}Cr_{12}Ni_{10}B_{15}WC_5$ are deposited on SS316L substrate using laser cladding technique a then the same have been studied to determine the influence of various compositions on wear property. Various characterization techniques such as scanning electron microscopy (SEM), EDX, and XPS have been used for microstructural analysis of the formed alloys.

Substrate and coating techniques

The base material used on which the coating is applied is SS316L which is 10 mm thick, with a square shape of 25 mm x 25 mm dimensions. The surface of the sample is ground using different sizes of sandpapers and finally mirror polished. After polishing the surface of the base metal is cleaned up by dilute hydrochloric acid and dried with cold air to remove any adhered substances. The powders of very high purity of iron, molybdenum, chromium, boron, tungsten, and carbide are mechanically mixed in different non-atomic ratios. The mixture is then used for coating using a laser cladding process. The deposition of the coating on the substrate was carried out at Industry Magod Fusion, Pune (Maharashtra, India). As mentioned above three different alloys have been prepared using different ratios of the powders and deposited on the substrate. The alloys mixtures using different percentages of boron and tungsten carbide have been used for making of these alloys and these are $Fe_{43}Mb_{15}Cr_{12}Ni_{10}B_7WC_{13}$, $Fe_{43}Mb_{15}Cr_{12}Ni_{10}B_{11}WC_9$, and $Fe_{43}Mb_{15}Cr_{12}Ni_{10}B_{15}WC_5$. The process parameters were selected such that there is minimum porosity in the alloying material and the substrate considered for better coating properties with minimum porosity.

Results and Discussion

Coating characterization

Figure 1a shows the SEM image of the composition in which the percentage addition of boron and tungsten carbide is 7% and 13%, respectively. This image represents the coating thickness with negligible porosity. The coating thickness is 1.776 mm, which tells the composite alloy binds well with the substrate. EDX spectrum is shown in figure 1b of $Fe_{43}Mo_{15}Cr_{12}Ni_{10}B_7WC_{13}$ to find out the formation of composite alloys. During the EDX analysis, many areas are focused and related peaks are shown. In the spectrum, the peaks of iron, molybdenum, chromium, boron, tungsten, and carbide are shown at different energy levels which ensures the presence of all elements on the base metal SS316L. In figure 1c, the percentage of boron and tungsten carbide is 11% and 9% where the coating thickness is 1.496 mm which shows the presence of composite at micron level on substrate. It has minimum porosity. Figure 1d represents the energy spectrum of $Fe_{43}Mo_{15}Cr_{12}Ni_{10}B_{11}WC_9$ in which the presence of elements can be identified through peaks present in the spectrum. Boron and tungsten have atomic percentage of 32.7% and 0.1% in the EDX spectrum analysis.

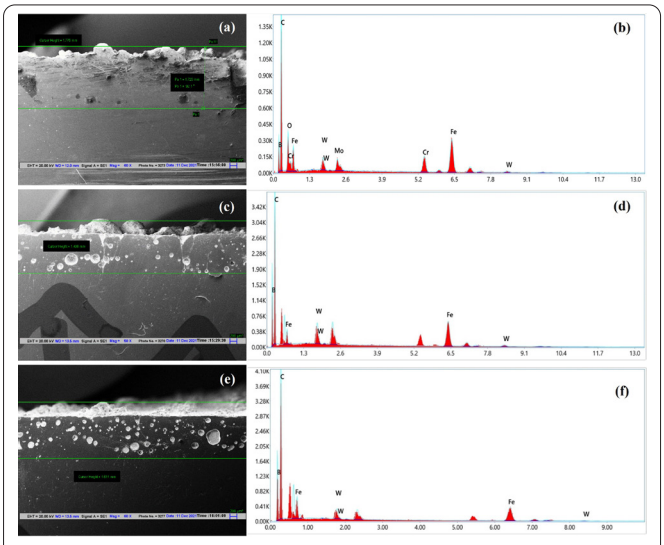

Figure 1: SEM and EDX image of composition **(a, b)** $Fe_{43}Mb_{15}Cr_{12}Ni_{10}B_7WC_{13}$, **(c, d)** $Fe_{43}Mb_{15}Cr_{12}Ni_{10}B_7WC_9$, and **(e, f)** $Fe_{43}Mb_{15}Cr_{12}Ni_{10}B_7WC_5$.

SEM image of coating thickness where the presence of boron and tungsten carbide is 15% and 5%. The thickness of the composite $Fe_{43}Mo_{15}Cr_{12}Ni_{10}B_{15}WC_5$ is 1.611 mm. The thickness value in every composition shows the strength of coating on SS316L. SEM images of coating thickness shows a little increase in hardness. Increase in hardness reflects the effect of laser speed of powder particles during the laser cladding deposition technique.

Microstructural analysis

XRD

XRD patterns show a modified crystallization sequence for the prepared composition (Figure 2). It reflects the coating has body center cubic (bcc) + fcc phase. When the percentage of boron and tungsten carbide is 7% and 13%, an evident diffraction peak appears with a phase of Fe_2O_3. While the other peaks also show the presence of other element through different symbols while the crystallinity of oxides MoO_2 with a crystal system orthorhombic, NiO_2, Cr_2O_3, and B_2O_3 with a crystal phase trigonal, there are various peaks at which three to four element oxides are present that can be seen in XRD pattern at different 2 theta (2θ) angles.

The second composition where the presence of boron and tungsten carbide is 9% and 11%. The phase of this composition also has fcc + bcc. NiO_2 has monoclinic phase while Fe_2O_3 has cubic phase, and the phase of others elemental oxides are trigonal. There are some peaks where the present of iron oxides, chromium oxides, and boron oxides are present together while on other peaks one element oxide or two element oxides are present.

The phase in the third composition is also amorphous with fcc + bcc phase if the percentage contribution of boron and tungsten carbide is 15% and 5%. The other phases are monoclinic, cubic, and trigonal for all elements oxides present in the composition $Fe_{43}Mb_{15}Cr_{12}Ni_{10}B_{15}WC_5$.

XPS

XPS analysis is a surface sensitive quantitative technique which uses photoelectric effect to analyze the presence of elements on the surface of the coated base metal. To achieve XPS analysis, sample size of 5 mm x 5 mm x 2 mm sample is prepared for all the three compositions $Fe_{43}Mb_{15}Cr_{12}Ni_{10}B_7WC_{13}$, $Fe_{43}Mb_{15}Cr_{12}Ni_{10}B_{11}WC_9$, and $Fe_{43}Mb_{15}Cr_{12}Ni_{10}B_{15}WC_5$.

Figure 3 shows the survey spectra of $Fe_{43}Mb_{15}Cr_{12}Ni_{10}B_7WC_{13}$ powder coated on SS316L. The required elements are present on the coated sample of SS316L. The formation of boron and carbon in B1s and C1s, respectively, showed the mixing of element powder with the substrate. The metalloid primary XPS region shows in B1s which highlights the variation of boron's presence. The value of intensity shows the bonding of boron which is 190 c/s when the binding energy is 192 eV. There are a lot of variations in peak in B1s that gives the idea of distribution of boron element across the surface area of the coated substrate.

In C1s XPS analysis, the variation is not present because

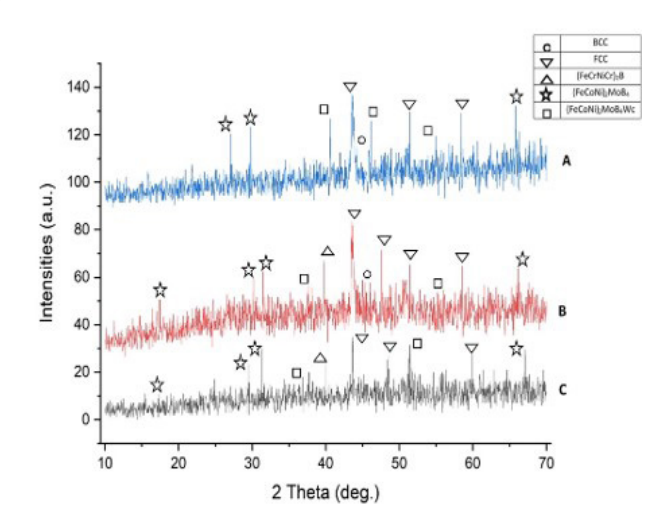

Figure 2: XRD patterns of non-equiatomic composite. **(a)** $Fe_{43}Mb_{15}Cr_{12}Ni_{10}B_7WC_{13}$, **(b)** $Fe_{43}Mb_{15}Cr_{12}Ni_{10}B_9WC_{11}$, and **(c)** $Fe_{43}Mb_{15}Cr_{12}Ni_{10}B_{15}WC_5$.

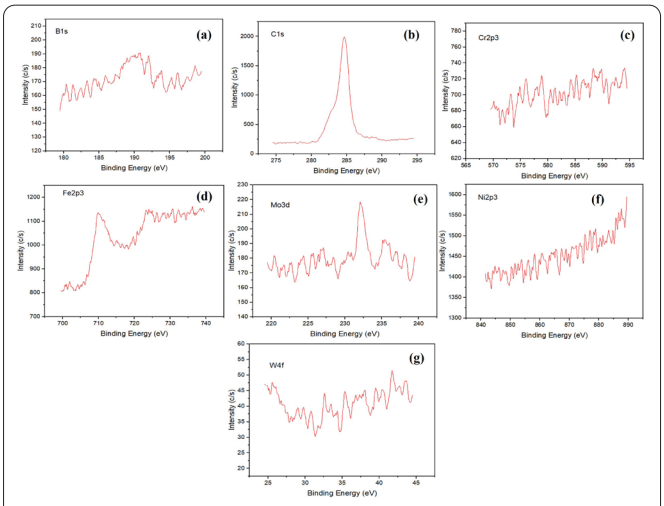

Figure 3: Survey spectra of **(a)** B1s, **(b)** C1s, **(c)** Cr2p3, **(d)** Fe2p3, **(e)** Mo3d, **(f)** Ni2p3, and **(g)** W4f of $Fe_{43}Mb_{15}Cr_{12}Ni_{10}B_7WC_{13}$ alloy.

the shape of the curve is bell shaped. The value of intensity and binding energy is different as compared to B1s. The peak is at 2000 c/s with a binding energy of 286 eV. In Cr2p3 XPS analysis, the binding energy is not as high as carbon. It means chromium is releasing its photo electrons to make a bond with the elements present on the surface as well as with SS316L. The configuration of Fe2p3 is also the same but the intensity count and binding energy is higher. In general, every element present on the surface is making a bond with the other elements and it shows the survey spectra of first composition on XPS.

If we see the XPS survey spectra of second composition $Fe_{43}Mb_{15}Cr_{12}Ni_{10}B_{11}WC_9$ in figure 4, it shows that the binding energy value for B1s is 182 eV which tells that the boron has less value of binding energy as compared other elements present on the base metal substrate. The variation in peak suggests that the boron is well distributed across the surface area of the coating. The XPS spectra of other elements are also shown in

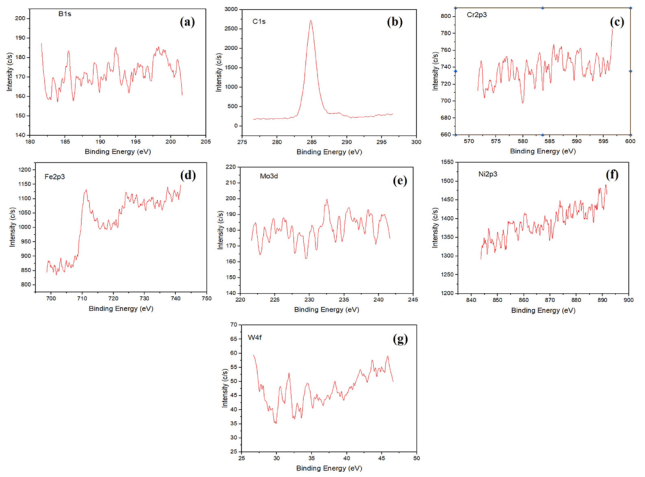

Figure 4: XPS survey spectra of second composition $Fe_{43}Mb_{15}Cr_{12}Ni_{10}B_{11}WC_9$ of **(a)** B1s, **(b)** C1s, **(c)** Cr2p3, **(d)** Fe2p3, **(e)** Mo3d, **(f)** Ni2p3, and **(g)** W4f of $Fe_{43}Mb_{15}Cr_{12}Ni_{10}B_7WC_9$ alloy.

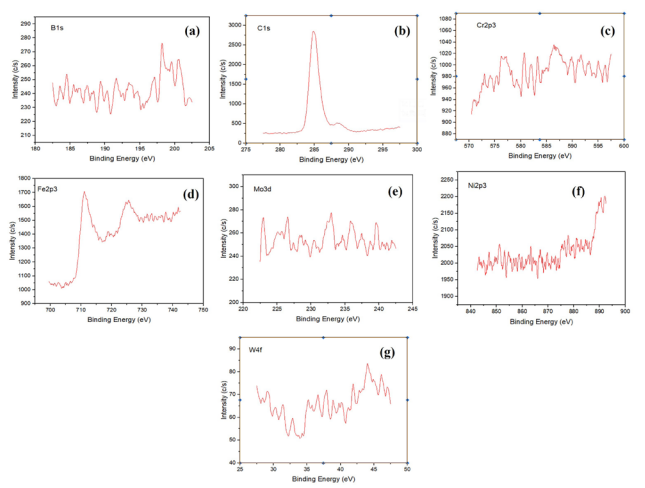

Figure 5: XPS third and final composition $Fe_{43}Mb_{15}Cr_{12}Ni_{10}B_{11}WC_9$ of **(a)** B1s, **(b)** C1s, **(c)** Cr2p3, **(d)** Fe2p3, **(e)** Mo3d, **(f)** Ni2p3, and **(g)** W4f of $Fe_{43}Mb_{15}Cr_{12}Ni_{10}B_7WC_5$ alloy.

figure 4 which gives the analysis of binding energy against the intensity. The variation in peaks of the elements gives the idea of distribution of the elements like iron, chromium, molybdenum, and tungsten carbide on the surface of SS316L substrate.

In the third and final composition $Fe_{43}Mb_{15}Cr_{12}Ni_{10}B_{15}WC_5$, the value of binding energy for B1s is 198 eV (Figure 5) which means the electrons are not easily leaving the nucleus of its element. But the variation in peaks shows the better distribution across the surface area. The XPS spectra of other elements is not much different if we compare it with the first two compositions. This tells that all the element powders are well mixed and have homogeneous coating on the base substrate SS316L.

Conclusions

Based on the above experiment, the following conclusions have been made:

- Microstructural behavior of $Fe_{43}Mn_{15}Cr_{12}Ni_{10}B_7WC_{13}$, $Fe_{43}Mn_{15}Cr_{12}Ni_{10}B_{11}WC_9$, and $Fe_{43}Mn_{15}Cr_{12}Ni_{10}B_{15}WC_5$ represents that the variation in percentage of boron and tungsten carbide improves the mechanical properties like wear resistance, strength of the coated metal, and corrosive resistance.
- EDX images show the presence of an element on the surface of coated metal. The images reflect the binding force of metal powders on the coated sample.
- SEM images of the compositions give the mixing of powders and cladded well on the substrate. While the XRD pattern shows the complex diffraction pattern of the compositions. The nature of crystallinity is amorphous with fcc + bcc phase.
- Through XPS, we can suggest that the binding strength of the element powders with the substrate is high which tells that it has good wear and corrosion resistance property.

Acknowledgements

None.

Conflict of Interest

None.

References

1. Nair RB, Selvam K, Arora HS, Mukherjee S, Singh H, et al. 2017. Slurry erosion behavior of high entropy alloys. *Wear* 386: 230-238. https://doi.org/10.1016/j.wear.2017.01.020
2. Lin MC, Chang LS, Lin HC, Yang CH, Lin KM. 2006. A study of high-speed slurry erosion of NiCrBSi thermal-sprayed coating. *Surf Coat Technol* 201(6): 3193-3198. https://doi.org/10.1016/j.surfcoat.2006.06.040
3. Thakur L, Arora N, Jayaganthan R, Sood R. 2011. An investigation on erosion behavior of HVOF sprayed WC–CoCr coatings. *Appl Surf Sci* 258(3): 1225-1234. https://doi.org/10.1016/j.apsusc.2011.09.079
4. Sharma P, Dwivedi VK, Dwivedi SP. 2021. Development of high entropy alloys: a review. *Mater Today Proc* 43: 502-509. https://doi.org/10.1016/j.matpr.2020.12.023
5. Hong S, Wu Y, Zheng Y, Wang B, Gao W, et al. 2014. Effect of spray parameters on the corrosion behavior of HVOF sprayed WC-Co-Cr coatings. *J Mater Eng Perform* 23: 1434-1439. https://doi.org/10.1007/s11665-014-0865-3
6. Bai Y, Xi Y, Gao K, Yang H, Pang X, et al. 2019. Brittle coating effects on fatigue cracks behavior in Ti alloys. *Int J Fatigue* 125: 432-439. https://doi.org/10.1016/j.ijfatigue.2019.04.017
7. Cho YS, Liao LK, Hsu CH, Hsu YH, Wu WY, et al. 2019. Effect of substrate bias on biocompatibility of amorphous carbon coatings deposited on Ti6Al4V by PECVD. *Surf Coat Technol* 357: 212-217. https://doi.org/10.1016/j.surfcoat.2018.09.070
8. Leech PW. 2014. Laser surface melting of a complex high alloy steel. *Mater Des* 54: 539-543. https://doi.org/10.1016/j.matdes.2013.08.060
9. Nair AM, Muvvala G, Nath AK. 2019. A study on in-situ synthesis of TiCN metal matrix composite coating on Ti–6Al–4V by laser surface alloying process. *J Alloys Compd* 810: 151901. https://doi.org/10.1016/j.jallcom.2019.151901
10. Spadaro L, Hereñú S, Strubbia R, Rosas GG, Bolmaro R, et al. 2020. Effects of laser shock processing and shot peening on 253 MA austenit-

ic stainless steel and their consequences on fatigue properties. *Opt Laser Technol* 122: 105892. https://doi.org/10.1016/j.optlastec.2019.105892

11. Wang Z, Zhang Q, Bagheri R, Guo P, Yao Y, et al. 2019. Influence of laser surface remelting on microstructure and degradation mechanism in simulated body fluid of Zn-0.5 Zr alloy. *J Mater Sci Technol* 35(11): 2705-2713. https://doi.org/10.1016/j.jmst.2019.05.019
12. Soleimanipour Z, Baghshahi S, Shoja-razavi R. 2017. Improving the thermal shock resistance of thermal barrier coatings through formation of an in situ YSZ/Al_2O_3 composite via laser cladding. *J Mater Eng Perform* 26: 1890-1899. https://doi.org/10.1007/s11665-017-2591-0
13. Wang S, Zhu L, Fuh JYH, Zhang H, Yan W. 2020. Multi-physics modeling and Gaussian process regression analysis of cladding track geometry for direct energy deposition. *Opt Lasers Eng* 127: 105950. https://doi.org/10.1016/j.optlaseng.2019.105950
14. Zhou S, Dai X, Zeng X. 2009. Effects of processing parameters on structure of Ni-based WC composite coatings during laser induction hybrid rapid cladding. *Appl Surf Sci* 255(20): 8494-8500. https://doi.org/10.1016/j.apsusc.2009.05.161
15. Li M, Han B, Song L, He Q. 2020. Enhanced surface layers by laser cladding and ion sulfurization processing towards improved wear-resistance and self-lubrication performances. *Appl Surf Sci* 503: 144226. https://doi.org/10.1016/j.apsusc.2019.144226
16. Liu C, Li C, Zhang Z, Sun S, Zeng M, et al. 2020. Modeling of thermal behavior and microstructure evolution during laser cladding of AlSi10Mg alloys. *Opt Laser Technol* 123: 105926. https://doi.org/10.1016/j.optlastec.2019.105926
17. Majumdar JD, Galun R, Mordike BL, Manna I. 2003. Effect of laser surface melting on corrosion and wear resistance of a commercial magnesium alloy. *Mater Sci Eng A* 361(1-2): 119-129. https://doi.org/10.1016/S0921-5093(03)00519-7
18. Li Z, Pradeep KG, Deng Y, Raabe D, Tasan CC. 2016. Metastable high-entropy dual-phase alloys overcome the strength–ductility trade-off. *Nature* 534(7606): 227-230. https://doi.org/10.1038/nature17981
19. Li Z, Tasan CC, Springer H, Gault B, Raabe D. 2017. Interstitial atoms enable joint twinning and transformation induced plasticity in strong and ductile high-entropy alloys. *Sci Rep* 7(1): 40704. https://doi.org/10.1038/srep40704